Dynamic Biochemical and Cellular Models of Bone Physiology: Integrating Remodeling Processes, Tumor Growth, and Therapy

Rui M. Coelho, Joana P. Neto, Duarte Valério and Susana Vinga

Abstract Bone is an active connective tissue composed of different types of cells. The dynamic behavior of bone remodeling processes is typically represented through differential equations, which represent the physiological phenomena occurring in this organ. These models take into account the tight biochemical regulation between osteoclasts and osteoblasts and have also been enriched with variables and parameters related to bone pathologies and treatment. This chapter reviews some of the more recent models describing bone physiology, focusing on those that include the main cellular processes, along the biochemical control, and also the pharmacokinetic/pharmacodynamic (PK/PD) of the most common treatments for diseases such as cancer. These models are then compared in terms of the simulations obtained and, finally, some highlights on integrating them with the biomechanical component of the system which will be given. These models are expected to provide a valuable insight into this complex system and to support the development of clinical decision systems for bone pathologies.

R. M. Coelho · D. Valério
IDMEC, Instituto Superior Técnico, Universidade de Lisboa, Av. Rovisco Pais 1, 1049-001 Lisbon, Portugal
e-mail: rui.coelho@tecnico.ulisboa.pt

D. Valério
e-mail: duarte.valerio@tecnico.ulisboa.pt

J. P. Neto
Instituto Superior Técnico, Universidade de Lisboa, Av. Rovisco Pais 1, 1049-001 Lisbon, Portugal
e-mail: joana.neto@tecnico.ulisboa.pt

S. Vinga (✉)
INESC-ID, Instituto Superior Técnico, Universidade de Lisboa, Av. Rovisco Pais 1, 1049-001 Lisbon, Portugal
e-mail: susanavinga@tecnico.ulisboa.pt

© Springer Nature Switzerland AG 2020

J. Belinha et al. (eds.), *The Computational Mechanics of Bone Tissue*,
Lecture Notes in Computational Vision and Biomechanics 35,
https://doi.org/10.1007/978-3-030-37541-6_4

Overview

This chapter reviews some of the most recent models of bone remodeling processes, focusing on those that include known biochemical phenomena. These models are then complemented with variables related to healthy and pathological states, namely to study oncological processes and other bone pathologies. Additionally, they have been enriched with therapy, by including the pharmacokinetics (PK) and pharmacodynamics (PD) of several bone treatments.

The main goal of the present review is to compare these approaches and highlight future directions, in particular, how these models can be integrated with biomechanical knowledge to build integrated models for bone physiology.

To better understand the mentioned models, this chapter follows a growing complexity hierarchy. Firstly, basic physiology concepts are introduced in Sect. 1, ranging from healthy bone dynamics to existing treatments for tumors in its microenvironment. Local mathematical and computational models are then presented (Sect. 2), followed by their non-local adaptations (Sect. 3). Different models are reviewed and pertinent simulations results are presented, from the simplest one involving only three state variables to more complex ones that include other physiological processes and therapy.

1 Bone Remodeling Physiology

Modeling complex physiological systems are gaining an increasing interest in engineering due to the expected impact in clinical sciences. These multidisciplinary fields are promoting the 4P approach to medicine, which is becoming more predictive, personalized, preventive, and participatory [15].

In particular, there are now many efforts to model bone physiology, taking into account all the biochemical, cellular, and environmental processes. However, for an accurate modeling process, the inherent physiology must be known.

1.1 Healthy Bone Remodeling

Living tissue is constantly being renovated, and this process is also true for bone tissue. Static as it may seem to the naked eye, bone undergoes a constant remodeling process, being resorbed by cells termed *osteoclasts* and formed by cells called *osteoblasts*. They constitute part of a BMU, a basic multicellular unit.

- **Osteoclasts**—Originated from the fusion of mononucleated cells and progenitor cells that express receptor activator of NF-κB (RANK) and macrophage colony-stimulating factor receptor (c-FMS), and osteoclasts differentiate into multinucleated cells when colony-stimulating factor 1 (CSF1) and RANK-ligand (RANKL) are present in the bone microenvironment. Being capable of bone resorption, their

generation rate determines the BMU extension; whereas, the life span determines the depth of resorption [3, 35].

- **Osteoblasts**—Osteoblasts are mononucleated cells able to form bone. They can regulate bone resorption and formation through parathyroid hormone (PTH) receptors and RANKL and osteoprotegerin (OPG) production. OPG is a soluble decoy receptor for RANKL that binds to RANK in osteoclasts precursors, consequently inhibiting osteoclast formation. Osteoblasts upregulate RANKL expression due to PTH, thus promoting their activation. PTH also contributes to osteoclastogenesis by decreasing the OPG production. The bone resorption and formation are regulated greatly by the RANK/RANKL/OPG pathway and PTH [10, 35].
- **Basic Multicellular Unit**—Basic multicellular units (BMU) are temporary anatomical structures, where autocrine and paracrine factors produced by osteoblasts and osteoclasts regulate the formation and activation of these cells. Bone resorbing osteoclasts lead an active BMU, removing old and damaged tissue. Osteoblasts then follow, occupying the tail portion of the BMU, secreting and depositing bone [33, 38].

Bone remodeling cycles can be activated by either mechanical *stimuli* on the bone, or through the production of estrogen or PTH [33] due to changes in homeostasis. The resorption phase is triggered by this hormone, which acts on cells of the osteoblastic lineage and leads to the differentiation and activation of osteoclasts. Active osteoclasts are then capable of degrading bone. At the resorpted site, the undigested demineralized collagen matrix is removed during the reversal phase, in preparation for bone formation. Then, osteoblasts form bone and replace the resorpted bone by the same amount, ending the bone remodeling cycle. The processes that link bone resorption to the initiation of bone formation may involve the release of coupling factors from bone during resorption phase, such as insulin growth factor I and II (IGF I and II) and transforming growth factor β (TGF-β), which attract osteoblasts to the sites of bone resorption [17]. Some of these processes are illustrated in Fig. 1.

1.2 Tumor in the Bone Remodeling Cycle

The previous section describes the main biochemical processes in healthy bone. When some pathology is present, the dynamic behavior of bone remodeling is severely affected, which usually disrupts its biochemical regulation and has a high impact on bone integrity. For example, in diseases such as cancer, either in bone tumors or through metastization of other primary tumors (e.g., breast or prostate cancer), the bone microenvironment is changed, affecting the osteoclasts/osteoblasts equilibrium. This leads, consequently, to bone lesions. Such pathophysiology is mostly explained by the theory of the vicious cycle proposed by Mundy and Guise in [14], according to which cancer cells resident in the bone can cause its destruction by stimulating osteoclast activity and receiving, in return, positive feedback from humoral factors released by the bone microenvironment during bone destruction [5].

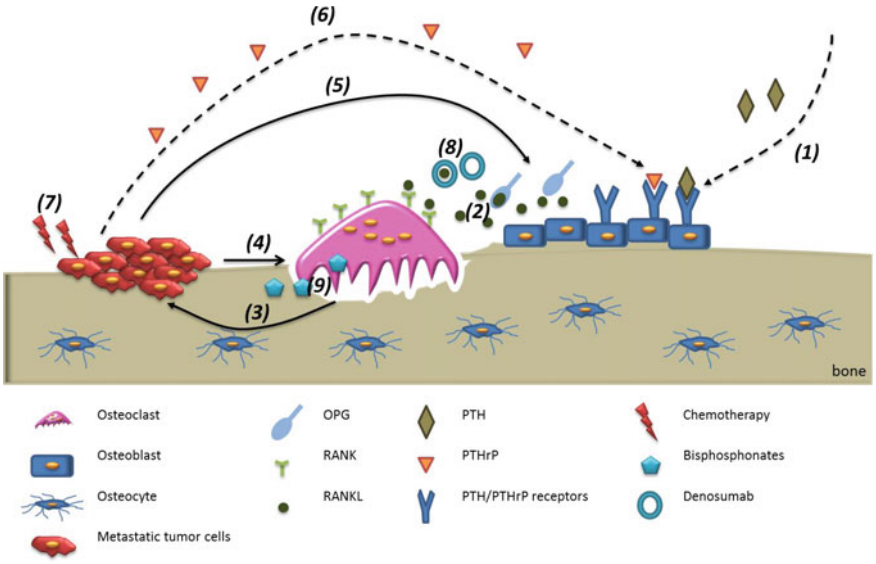

Fig. 1 Biochemical processes of bone remodeling, progression of bone metastases and treatment. Bone remodeling: (1) PTH stimulates RANKL production by osteoblasts; (2) RANK/RANKL/OPG pathway plays an important role in bone resorption and formation; bone metastases vicious cycle: (3) Bone-derived tumor growth factors (IGFs,TGF-β, bone morphogenetic protein (BMP), among others); (4) Tumor-derived factors stimulate bone resorption (parathyroid hormone-related protein (PTHrP), TGF-β, IL-8,11, among others); (5) Tumor-derived factors affect bone formation (DKK1, BMP, IGFs, among others); (6) PTHrP stimulates RANKL production by osteoblasts treatment: (7) Chemotherapy directly targets cancer cells; (8) Denosumab binds to RANKL, inhibiting osteoclast formation; (9) Bisphosphonates promote osteoclast apoptosis. Reprinted from [9]: Journal of Theoretical Biology, Vol 391, Coelho et al., Dynamic modeling of bone metastasis, microenvironment and therapy. Integrating parathyroid hormone (PTH) effect, anti-resorptive and anti-cancer therapy, Pages No. 1–12.Copyright 2016, with permission from Elsevier

Bone metastases can be osteolytic, in case bone resorption is increased, or osteoblastic, when bone formation is stimulated in an unstructured way. Both bone resorption and formation are still present in any case, although out of balance, resulting in loss of bone resistance and integrity. Breast cancer metastases are prone to develop osteolytic metastasis, and prostate cancer ones are usually osteoblastic [44].

For the bone remodeling deregulation resulting from *osteolytic* metastases, metastatic cells stimulate bone resorption [7], and TGF-β is released from the bone matrix, during bone resorption. TGF-β stimulates tumor growth and parathyroid hormone-related protein (PTHrP) production in metastatic cells that binds to PTH receptors on cells of osteoblastic lineage. RANKL levels are then enhanced, and, subsequently, osteoclasts are activated, leading to increased bone resorption [5]. Osteoclasts activity, in turn, will result in the release of TGF-β from the degraded bone, which further stimulates tumor growth and PTHrP secretion, giving rise to a vicious cycle.

In *osteoblastic* metastases, tumorous cells grow, as bone expresses endothelin-1 (ET-1) that stimulates osteoblasts through the endothelin A receptor (ETR), activating Wnt signaling. Tumor-derived proteases contribute to the release of osteoblastic factors from the extracellular matrix, including TGF-β and IGF I. RANKL is increased due to tumor-induced osteoblast activity, leading to the release of PTH and promoting osteoclast activity [5]. Thus, the tumor microenvironment leads to the accumulation of newly formed bone.

Although the reviewed models are mostly focused on cancer, these can be easily adapted to other bone pathologies. Such can be found in [41], where the model in [42] is extended to enable the simulation of postmenopausal osteoporosis effects on bone remodeling combined with the pharmacodynamical effects of drug treatment denosumab. Also, in [19], the original model in [17] is adapted to account for the effect of osteomyelitis, a bone pathology caused by bacteria infection (mostly *Staphylococcus aureus*), which alters the RANK/RANKL/OPG signaling dynamics that regulates osteoblasts and osteoclasts behavior in bone remodeling.

1.3 Bone Treatments

There are several possible targets for bone metastases treatment, as detailed in review [6], namely bone resorption, osteoblast, and tumor cells.

Anti-resorptive treatment targets osteoclasts, since these cells are essential to the vicious cycle of bone metastases. For osteolytic metastases, such as those from breast cancer, bisphosphonates or denosumab treatment is administrated as effective anti-resorptive therapies [5]. While bisphosphonates lodge in bone and poison osteoclasts as they degrade bone, denosumab, a fully human monoclonal antibody binds exclusively to RANKL, inhibiting osteoclast formation.

Although therapeutics that targets osteoblasts exists, such as PTH daily administration or endothelin, these are far less well-developed and used than anti-resorptive therapy, in order to decrease tumor burden on bone and recover bone mass.

Anti-cancer agents that target metastatic cells directly, such as chemotherapy and hormone therapy [22] should be used in combination with the other presented therapies.

2 Mathematical Bone Remodeling Local Models

Computational models of the dynamics of bone remodeling and its interaction with cancer cells are important to simulate the biochemical processes occurring in the bone microenvironment that potentiate the progression of such disease. The importance of understanding such a complex systems is highlighted in [26], which presents a review of mathematical modeling methodologies, applied to bone biology.

In all that follows, we will use systems of differential equations where D^1 is a first-order derivative in order to time, $\frac{\mathrm{d}}{\mathrm{d}t}$.

2.1 Healthy Remodeling Dynamics

The simplest model of bone remodeling involves a system of three ordinary differential equations representing osteoclast and osteoblast densities and normalized bone mass [17]. In this early proposal, bone remodeling is represented as an S-system [40], described by Eqs. (1a)–(1c), coupling the behavior of osteoclasts, $C(t)$, and osteoblasts, $B(t)$, through biochemical autocrine (g_{CC}, g_{BB}) and paracrine (g_{BC}, g_{CB}) factors expressed implicitly in the exponents.

$$D^1 C(t) = \alpha_C C(t)^{g_{CC}} B(t)^{g_{BC}} - \beta_C C(t) \tag{1a}$$

$$D^1 B(t) = \alpha_B C(t)^{g_{CB}} B(t)^{g_{BB}} - \beta_B B(t) \tag{1b}$$

$$D^1 z(t) = -k_C \max\{0, C(t) - C_{ss}\} + k_B \max\{0, B(t) - B_{ss}\} \tag{1c}$$

This is a local model that only takes into account temporal dynamics and whose variables and typical parameters values used in the simulations are described in the Table 3. It is worth noting that the RANK/RANKL/OPG pathway is implicitly encoded as their ratio is in the osteoblasts-derived osteoclasts paracrine regulator, g_{BC}. The constants $\alpha_{C,B}$ and $\beta_{C,B}$ represent the activation and apoptosis rate, respectively, of the corresponding cell type. Bone resorption from active osteoclasts and bone formation from active osteoblasts command the temporal evolution of the bone mass, z, through the rates k_C and k_B, respectively. The action of each cell type $C(t)$ and $B(t)$ is considered only when its number is above its steady-state values C_{ss} and B_{ss} (Eqs. 2a–2c).

$$C_{ss} = \left(\frac{\beta_C}{\alpha_C}\right)^{\frac{(1-g_{BB})}{\Gamma}} \left(\frac{\beta_B}{\alpha_B}\right)^{\frac{g_{BC}}{\Gamma}} \tag{2a}$$

$$B_{ss} = \left(\frac{\beta_C}{\alpha_C}\right)^{\frac{g_{CB}}{\Gamma}} \left(\frac{\beta_B}{\alpha_B}\right)^{\frac{(1-g_{CC})}{\Gamma}} \tag{2b}$$

$$\Gamma = g_{CB} g_{BC} - (1 - g_{CC})(1 - g_{BB}) \tag{2c}$$

By setting the values of the exponents appropriately, in particular g_{BC}, this model is capable of describing a single remodeling cycle or a periodic behavior, whose amplitude and frequency of oscillations depend on the initial conditions, as can be seen in Figs. 2 and 3, respectively. The parameters used in these simulations are those from the values in column *A* of Table 3, except those explicitly defined in the caption of the figures, in accordance with [17].

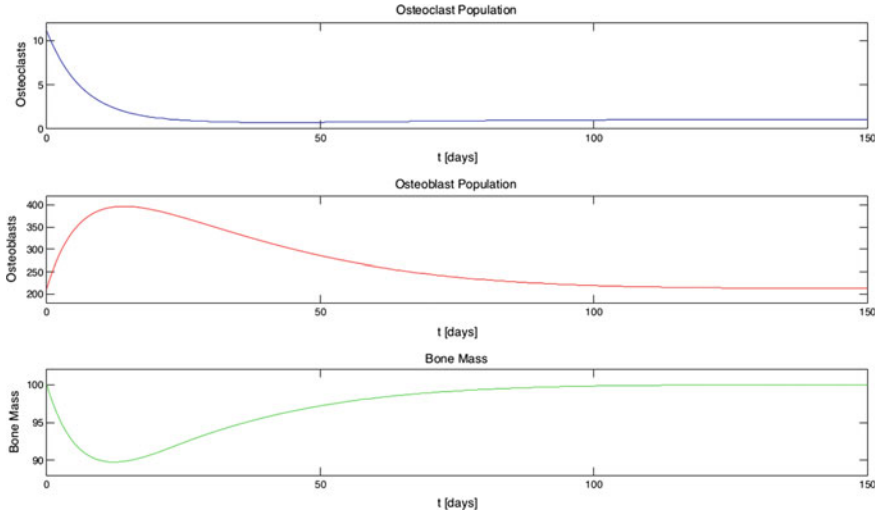

Fig. 2 Simulation of the model in Eqs. (1a)–(1c): number of osteoclasts, osteoblasts, and bone mass during normal bone modeling for a *single event*, triggered by an increase of the osteoclast population. The parameters are those in column *A* of Table 3 [2]

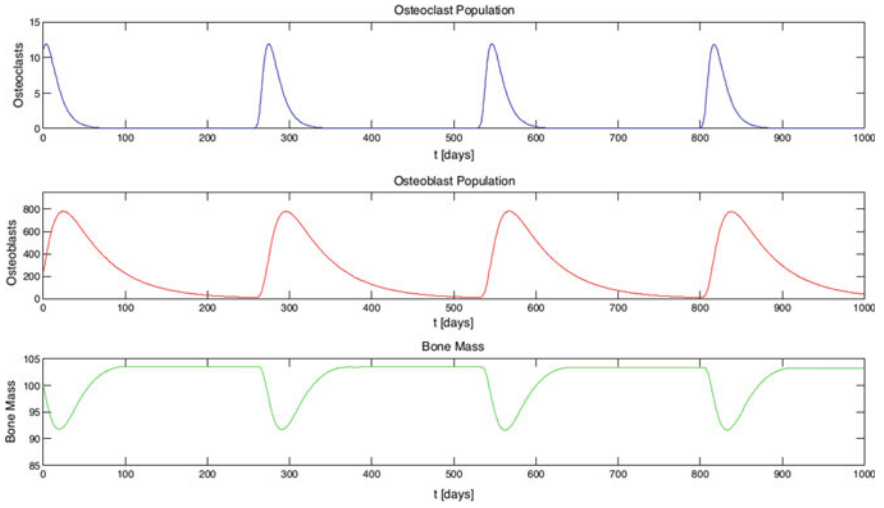

Fig. 3 Simulation of *oscillatory changes* in the number of osteoclasts, osteoblasts, and bone mass during normal bone remodeling for which the model presented in [17] has periodic solutions. Such behavior was triggered with an increase of ten units of the steady-state osteoclast population, $C_0 = 11.16$ and $C_{th} = 1.16$. The parameters were set according to [2]: $g_{CC} = 1.1$, being the responsible for the bone dynamic response, $\kappa_C = 0.0748$, $\kappa_B = 6.3952 \times 10^{-4}$ and $B_0 = B_{th} = 231.72$. Other parameters were set according to column *A* of Table 3

Due to its simplicity and versatility, this model serves as a basis for many other studies. In [16], the anabolic and catabolic effects of external administration of PTH on bone remodeling are studied, by using the single remodeling cycle behavior exhibited in [17]. The influence of PTH in the production of RANKL by osteoblasts is encoded in the exponent g_{BC}, adding a pulse of fixed duration at a specific time. The duration of application of PTH influences qualitatively the bone mass outcome and can be used to achieve different scenarios of bone modeling. It is possible to apply bifurcation analysis to generalized bone models [50], in particular to the model in [17], adding the osteoblasts precursors to the system. A stability analysis is hence achieved for this type of models.

More recently, the integration of PTH into the model was proposed [9], as given by Eqs. (3a)–(3e).

$$D^1 C(t) = \alpha_C C(t)^{g_{CC}} B(t)^{g_{BC} + K_{\mathrm{PTH}_{\mathrm{pool}}BC} \mathrm{PTH}_{\mathrm{pool}}(t)} - \beta_C C(t), \tag{3a}$$

$$D^1 B(t) = \alpha_B C(t)^{g_{CB}} B(t)^{g_{BB}} - \beta_B B(t), \tag{3b}$$

$$D^1 \mathrm{PTH}_{\mathrm{pool}}(t) = -\beta_{\mathrm{PTH}} \mathrm{PTH}_{\mathrm{pool}}(t) + K_{\mathrm{PTH}} \delta(t), \tag{3c}$$

$$P(\delta(t) = 1) = 1 - \exp\left(-\left(\frac{t}{\lambda_W}\right)^{k_W}\right), \tag{3d}$$

$$D^1 z(t) = -k_C \max\{0, C(t) - C_{ss}\} + k_B \max\{0, B(t) - B_{ss}\}, \tag{3e}$$

The PTH concentration is included in $\mathrm{PTH}_{\mathrm{pool}}(t)$, and $\delta(t)$ represents a train of Dirac deltas, occurring stochastically with a Weibull distribution with probability P given by Eq. (3d). K_{PTH} is the increase of $\mathrm{PTH}_{\mathrm{pool}}(t)$ with each Dirac delta. This increase in PTH concentration is responsible for initiating a single remodeling cycle, which increases the production of RANKL by osteoblasts, thus affecting g_{BC}, as in Eq. (3a). Variable $K_{\mathrm{PTH}_{\mathrm{pool}}BC}$ quantifies this influence on the RANKL/OPG ratio. [13] further extends the model in [17] to include osteocytes and pre-osteoblasts in the bone model, predicting an osteocyte-induced bone remodeling after apoptosis. The role of sclerostin is also included, enabling the study of anti-sclerostin drugs in bone turnover.

Lemaire et al. [18] present a different approach, incorporating explicitly the RANK/RANKL/OPG pathway, TGF-β, and PTH in the model. The kinetic reactions of these molecules can activate or repress mechanisms of differentiation and activation of bone cells, here considered to be the uncommitted osteoblast precursors B_u, osteoblast precursors B_p, active osteoblasts B_a, and active osteoclasts C_a. This model serves as the basis to [27], whose model is presented in Eqs. (4a)–(4d).

$$D^1 B_p(t) = \alpha_{B_u} \pi^{\text{TGF-}\beta}_{\mathrm{act},B_u} - \alpha_{B_p} B_p(t) \pi^{\text{TGF-}\beta}_{\mathrm{rep},B_p} \tag{4a}$$

$$D^1 B_a(t) = \alpha_{B_p} B_p(t) \pi^{\text{TGF-}\beta}_{\mathrm{rep},B_p} - \beta_{B_a} B_a(t) \tag{4b}$$

$$D^1 C_a(t) = \alpha_{C_p} C_p \pi^{\mathrm{RANKL}}_{\mathrm{act},C_p} - \beta_{C_a} C_a(t) \pi^{\text{TGF-}\beta}_{\mathrm{act},C_p}, \tag{4c}$$

$$D^1 z = -k_C (C_a(t) - C_a(t_0)) + k_B (B_a(t) - B_a(t_0)) \tag{4d}$$

Functions $\pi^{\text{molecule}}_{\text{act/rep, cell}}$ represents activation (act) or repression (rep) of a given process in a cell type (cell) when binding to the molecule considered (molecule), and the corresponding coefficients are α_{cell}. It is usual to describe them as Hill functions, given by Eqs. (5a) and (5b), where X is the concentration of the molecule driving a cellular process, and K_1 and K_2 are activation or repression coefficients.

$$\pi^{X}_{\text{act}} = \frac{X}{K_1 + X} \tag{5a}$$

$$\pi^{X}_{\text{rep}} = \frac{1}{1 + X/K_2} \tag{5b}$$

Osteoblast precursors B_p differentiate from uncommitted osteoblast progenitors B_u at rate α_{B_u}, promoted by TGF-β. Osteoblast precursors differentiate into active osteoblasts B_a at rate α_{B_p}, inhibited by TGF-β. The number of active osteoblasts increases through this differentiation, but these cells have an apoptosis rate of β_{B_a}. The differentiation of osteoclasts precursors C_p into active osteoclasts C_a is promoted by RANKL, at rate α_{C_p}. TGF-β also promotes the apoptosis of active osteoclasts, occurring at rate β_{C_a}. It is assumed that the number of osteoclast precursors C_p and uncommitted osteoblast progenitors B_u is large and constant. The bone mass z is affected by bone resorption and formation, proportionally to the deviation from steady state of the number of active osteoclasts and osteoblasts, respectively. These cells are considered to be in their steady state at initial time t_0. Models for the concentrations of TGF-β and RANKL are proposed. The TGF-β release rate from the bone during resorption is proportional to the number of active osteoclasts. The RANK/RANKL/OPG pathway is explicitly modeled, including the influence of PTH on RANKL and OPG concentrations. The model is then studied for different scenarios, namely the importance of RANKL and OPG expression in the bone remodeling cycle. Moreover, the model parameter space is searched for physiologically sensible behaviors. In [28], the role of RANK/RANKL/OPG pathway is studied following the model in [27]. Furthermore, it was possible to simulate several bone diseases by changing the values of parameters, as well as different treatment strategies for these conditions, following the same approach.

2.2 Models Including Tumor Burden

Cancer interferes with the bone remodeling equilibrium, taking advantage of the dysregulated microenvironment to proliferate. Studying such alterations is important for cancers that begin in bone tissue, such as multiple myeloma, but also for bone metastases that often result from some kinds of cancer, such as breast or prostate cancer [44]. A modified version of the model in [17] which introduces multiple myeloma disease is presented in [2] and is described in Eqs. (6a)–(6d).

$$D^1C(t) = \alpha_C C(t)^{\left(g_{CC}\left(1+r_{CC}\frac{T(t)}{L_T}\right)\right)} B(t)^{\left(g_{BC}\left(1+r_{BC}\frac{T(t)}{L_T}\right)\right)} - \beta_C C(t), \tag{6a}$$

$$D^1B(t) = \alpha_B C(t)^{\left(\frac{g_{CB}}{1+r_{CB}\frac{T(t)}{L_T}}\right)} B(t)^{\left(g_{BB}-r_{BB}\frac{T(t)}{L_T}\right)} - \beta_B B(t), \tag{6b}$$

$$D^1T(t) = \gamma_T T(t) \log \frac{L_T}{T(t)}, \tag{6c}$$

$$D^1z(t) = -k_C \max\{0, C(t) - C_{ss_T}\} - k_B \max\{0, B(t) - B_{ss_T}\}, \tag{6d}$$

In this model, $T(t)$ represents tumor concentration and its growth; $D^1T(t)$ is made independent of the bone microenvironment, following a Gompertz law with growth rate γ_T and maximum size L_T, described by Eq. (6c). It affects the autocrine parameters in the exponents of the system through r_{CC} and r_{BB} and paracrine parameters through r_{BC} and r_{CB}, contributing to the increase in the number of osteoclasts and the decrease in osteoblasts when set to non-negative values. This results in the deregulation of the periodic remodeling cycles and, consequently, in the decrease of the overall bone mass. The equation for bone mass $z(t)$ keeps the same structure, although the thresholds to determine the number of active bone cells are no longer the steady states in healthy bone remodeling (C_{ss}, B_{ss}), but the steady states are (C_{ss_T}, B_{ss_T}) computed considering $T(t)$ to be at its maximum value L_T.

The model in [9], as presented in Eqs. (3a)–(3e), is extended in the same work to include the growth of bone metastasis and its influence on the bone microenvironment, described by Eqs. (7a)–(7g).

$$D^1C(t) = \alpha_C C(t)^{\left(g_{CC}+r_{CC}\frac{T(t)}{L_T}\right)} B(t)^{\left(g_{BC}+K_{\mathrm{PTH}_{\mathrm{pool}}\mathrm{BC}}\mathrm{PTH}_{\mathrm{pool}}(t)\right)} - \beta_C C(t), \tag{7a}$$

$$D^1B(t) = \alpha_B C(t)^{\left(\frac{g_{CB}}{1+r_{CB}\frac{T(t)}{L_T}}\right)} B(t)^{\left(g_{BB}-r_{BB}\frac{T(t)}{L_T}\right)} - \beta_B B(t), \tag{7b}$$

$$\begin{aligned} D^1\mathrm{PTH}_{\mathrm{pool}}(t) = {} & -\beta_{\mathrm{PTH}}\mathrm{PTH}_{\mathrm{pool}}(t) + K_{\mathrm{PTH}}\delta(t) \\ & + r_{\mathrm{PTHrP}} \max\{0, C(t) - C_{th}(t)\}\frac{T(t)}{L_T}, \end{aligned} \tag{7c}$$

$$P(\delta(t) = 1) = 1 - \exp\left(-\left(\frac{t}{\lambda_W}\right)^{k_W}\right), \tag{7d}$$

$$D^1T(t) = k_T \max\{0, C(t) - C_{th}(t)\}\frac{T(t)}{\lambda_T + T(t)}, \tag{7e}$$

$$D^1C_{th}(t) = \alpha_C C_{th}(t)^{\left(g_{CC}+r_{CC}\frac{T(t)}{L_T}\right)} B_{th}(t)^{g_{BC}} - \beta_C C_{th}(t), \tag{7f}$$

$$D^1B_{th}(t) = \alpha_B C_{th}(t)^{g_{CB}} B_{th}(t)^{\left(g_{BB}+r_{BB}\frac{T(t)}{L_T}\right)} - \beta_B B_{th}(t). \tag{7g}$$

Metastatic cells produce PTHrP in the presence of TGF-β, which is released from bone after bone resorption, encoded by the term $r_{\mathrm{PTHrP}} \max\{0, C(t) - C_{th}(t)\}\frac{T(t)}{L_T}$ in Eq. (7c). Osteoblasts have the same receptors for both PTH and PTHrP, which contribute to the production of RANKL. As such, PTHrP concentration is added to the

PTH_{pool} dynamics, which now includes PTH and PTHrP concentration. Increased production of RANKL means the number of osteoclasts will rise, resulting in an increased bone resorption. Bone resorption releases tumor growth factors from bone, allowing the tumor to grow, as described by Eq. (7e), and to produce PTHrP, which will, in turn, indirectly stimulate the activation of osteoclasts and bone resorption. As such, this model is able to describe the vicious cycle of bone metastases through the action of PTHrP. The growth rate of metastases includes a saturation term on the size of the tumor, introduced by a sigmoid function. As bone metastases $T(t)$ depend on growth factors released during bone resorption to grow, the dynamics for tumor growth is given by Eq. (7e), in which its growth rate due to tumor size is limited by a sigmoid function. Besides affecting the number of osteoclasts indirectly through PTH_{pool}, the tumor also affects the dynamics of the system through the autocrine parameters, as in [2]. In the presence of tumor, the thresholds for active osteoclasts and osteoblasts are no longer static C_{th} and B_{th}, since the steady state is affected thereby. Dynamic thresholds $C_{th}(t)$ and $B_{th}(t)$ are then used to determine the number of active cells, as given by Eqs. (7f) and (7g), respectively.

The bone remodeling model of [27] is extended in [49] to include the influence of multiple myeloma in the bone microenvironment. The explicit inclusion of IL-6 and multiple myeloma bone marrow stromal cell adhesion in the model, along with the multiple myeloma disease, made it possible to predict a vicious cycle between bone and multiple myeloma cells.

2.3 Introducing Treatment

2.3.1 Pharmacokinetics and Pharmacodynamics

The **pharmacokinetics** (PK) of a drug describes its concentration evolution at the target tissue; whereas, the effect of such concentration is given by **pharmacodynamics** (PD). A PK one-compartment model with first-order absorption and elimination for subcutaneous administration is described by Eqs. (8a) and (8b), where C_g is the drug concentration yet to be absorbed and C_p the concentration in the plasma [12]. The drug is absorbed at rate k_a and eliminated at rate k_e.

$$D^1 C_g(t) = -k_a C_g(t) \tag{8a}$$

$$D^1 C_p(t) = k_a C_g(t) - k_e C_p(t) \tag{8b}$$

$$C^0 = \frac{D_0 F}{V_d} \tag{8c}$$

The initial drug concentration C^0 can be computed from the initial administered dose D_0, the bioavailability F, and volume distribution V_d, following Eq. (8c). The plasma concentration can be described in the Laplace domain, $C_p(s)$ as Eq. (9), where s is the Laplace transform variable of time.

$$C_p(s) = C^0 \frac{k_a}{(s + k_a)(s + k_e)} \tag{9}$$

From Eq. (9), the time response for single-dose administration is ruled by Eq. (10).

$$C_p(t) = C^0 \frac{k_a}{k_a - k_e}(e^{-k_d t} - e^{-k_a t}) \tag{10}$$

For multiple dose administration, assuming that every dose initial concentration is C^0 and they are administrated at a constant time interval τ, the drug concentration after the nth dose is described by

$$C_p(n, t') = C^0 \frac{k_a}{k_a - k_e}\left(\frac{1 - e^{-nk_e\tau}}{1 - e^{-k_e\tau}} e^{-k_e t'} - \frac{1 - e^{-nk_a\tau}}{1 - e^{-k_a\tau}} e^{-k_a t'}\right) \tag{11}$$

where $t' = t - (n - 1)\tau$ represents the time elapsed after the n^{th} dose. For single intravenous (IV) administration, the PK is given by Eq. (12a), where the initial dose D_0 is included in the initial condition of C_p as Eq. (12b).

$$\frac{\mathrm{d}C_p(t)}{\mathrm{d}t} = -k_e C_p(t), \tag{12a}$$

$$C^0 = \frac{D_0}{V_d} \tag{12b}$$

In steady state, that is, after a large number of doses, the average concentration will be $\bar{C}_{p_{ss}} = \frac{1}{\tau}\frac{C^0}{k_e}$.

The effect of a drug $\mathrm{d}(t)$ according to its concentration in plasma C_p can be given by a Hill function as in Eq. (13), where an effect of 50% is achieved at concentration C_{50}.

$$\mathrm{d}(t) = \frac{C_p(t)}{C_{50} + C_p(t)} \tag{13}$$

The variables and parameters involved in the PK/PD model are summarized in Table 1.

2.3.2 Models for Tumor Treatment

The models proposed in [2] also allowed for tumor treatment. Since proteasome inhibitors are known to have direct anti-myeloma effects and to have direct effects on osteoblasts to stimulate osteoblast differentiation and bone formation, two time-dependent treatment step functions, $V_1(t)$ and $V_2(t)$, were introduced to model the inhibition of the osteoblasts apoptosis and tumor cells death, respectively. As such, Eqs. (6b) and (6c) are replaced by Eqs. (14a) and (14b), respectively, with $V_1(t)$ and $V_2(t)$ affecting the suitable parameters. This model including treatment is therefore

Table 1 Variables and parameters of the PK/PD model

Variable	Description	Units
$C_p(t)$	Effective drug concentration in the plasma	mg/L
$C_g(t)$	Concentration of drug remaining to be absorbed	mg/L
Parameter	Description	Units
C^0	Initial plasma concentration	mg/L
D_0	Drug dosage	mg
τ	Administration time interval	day
k_e	Drug elimination rate	day^{-1}
k_a	Drug absorption rate	day^{-1}
F	Bioavailability	–
V_d	Volume distribution	L
C_{50}	Drug concentration for 50% of maximum effect	mg/L

composed of Eqs. (6a), (14a), (14b), and (6d), resulting in an increase of bone mass and the elimination of tumor.

$$D^1 B(t) = \alpha_{_B} C(t)^{\left(\frac{g_{CB}}{1+r_{CB}\frac{T(t)}{L_T}}\right)} B(t)^{\left(g_{BB}-r_{BB}\frac{T(t)}{L_T}\right)} - \left(\beta_{_B} - V_1(t)\right) B(t) \tag{14a}$$

$$D^1 T(t) = \left(\gamma_{_T} - V_2(t)\right) T(t) \log\left(\frac{T(t)}{L_{_T}}\right) \tag{14b}$$

This work [9] also proposes the treatment of bone metastases through anti-cancer therapy and anti-resorptive therapy corresponding to the administration of either bisphosphonates or denosumab. Bisphosphonates (zoledronic acid) promote osteoclast apoptosis, and denosumab acts as a decoy receptor for RANKL, indirectly inhibiting osteoclast formation. Since both therapies act on osteoclasts, the effects of bisphosphonates, d_1, and denosumab, d_2, are included in Eq. (7a) as described in Eq. (15a). Chemotherapy (paclitaxel), whose effect is given by d_3, is considered for anti-cancer therapy, targeting metastatic cells directly, and so it is included in Eq. (7e) as shown in Eq. (15b). The treatment also affects the threshold for active osteoclasts, C_{th} , described by Eq. (15c). Including treatment variables, this new model is composed of Eqs. (15a), (7b), (7c), (7d), (15b), (15c), and (7g).

$$\begin{aligned} D^1 C(t) &= \alpha_{_C} C(t)^{g_{CC}+r_{CC}\frac{T(t)}{L_T}} B(t)^{g_{BC}+K_{\text{PTH}_{\text{pool}}BC}\,\text{PTH}_{\text{pool}}(t)-K_{d_1}d_1(t)} \\ &\quad - (\beta_{_C} + K_{d_2}d_2(t))C(t), \end{aligned} \tag{15a}$$

$$D^1 T(t) = k_{_T} \max\{0, C(t) - C_{th}(t)\}\frac{T(t)}{\lambda_T + T(t)} - K_{d_3}d_3(t)T(t), \tag{15b}$$

$$\begin{aligned} D^1 C_{th}(t) &= \alpha_{_C} C_{th}(t)^{g_{CC}+r_{CC}\frac{T(t)}{L_T}} B_{th}(t)^{g_{BC}-K_{d_1}d_1(t)} \\ &\quad - (\beta_{_C} + K_{d_2}d_2(t))C_{th}(t), \end{aligned} \tag{15c}$$

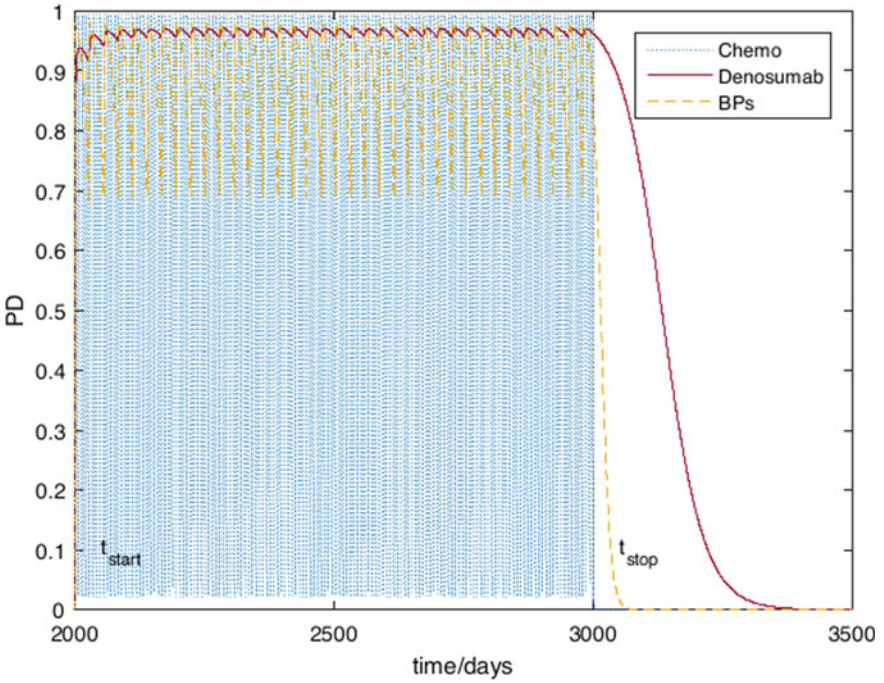

Fig. 4 PD effect of chemotherapy (paclitaxel), denosumab, and bisphosphonates (zoledronic acid), with administration parameters from Table 2 [9]

Table 2 Parameters for the therapy model (15), following [9]: denosumab, d_1; bisphosphonates, d_2 (zoledronic acid); anti-cancer therapy (paclitaxel), d_3

Parameter	d_1	d_2	d_3
D_0	120	4	176
τ	28	28	7
k_e	0.0248	0.1139	1.2797
k_a	0.2568	–	–
F	0.62	–	–
V_d	3.1508	536.3940	160.2570
C_{50}	1.2	0.0001	0.002
K_d	0.48	1.2	0.017

The PK/PD of denosumab (subcutaneous administration), zoledronic acid, and paclitaxel (both IV administration) is included in the model as described in Sect. 2.3.1. Figure 4 illustrates a simulation of the pharmacodynamics of these drugs, with administration starting at time $t_{\text{start}} = 2000$ days and interrupted at $t_{\text{stop}} = 3000$ days. The parameters for PK/PD are shown in Table 2. It is possible to observe that chemotherapy effect oscillates more than both drugs used for anti-resorptive therapy.

The treatment of bone metastases with chemotherapy alone and combined with either denosumab or bisphosphonates results in the dynamics shown in Figs. 5 and 6. The parameters used in the simulations are those from the values column *B* in Table 3, in accordance with [9].

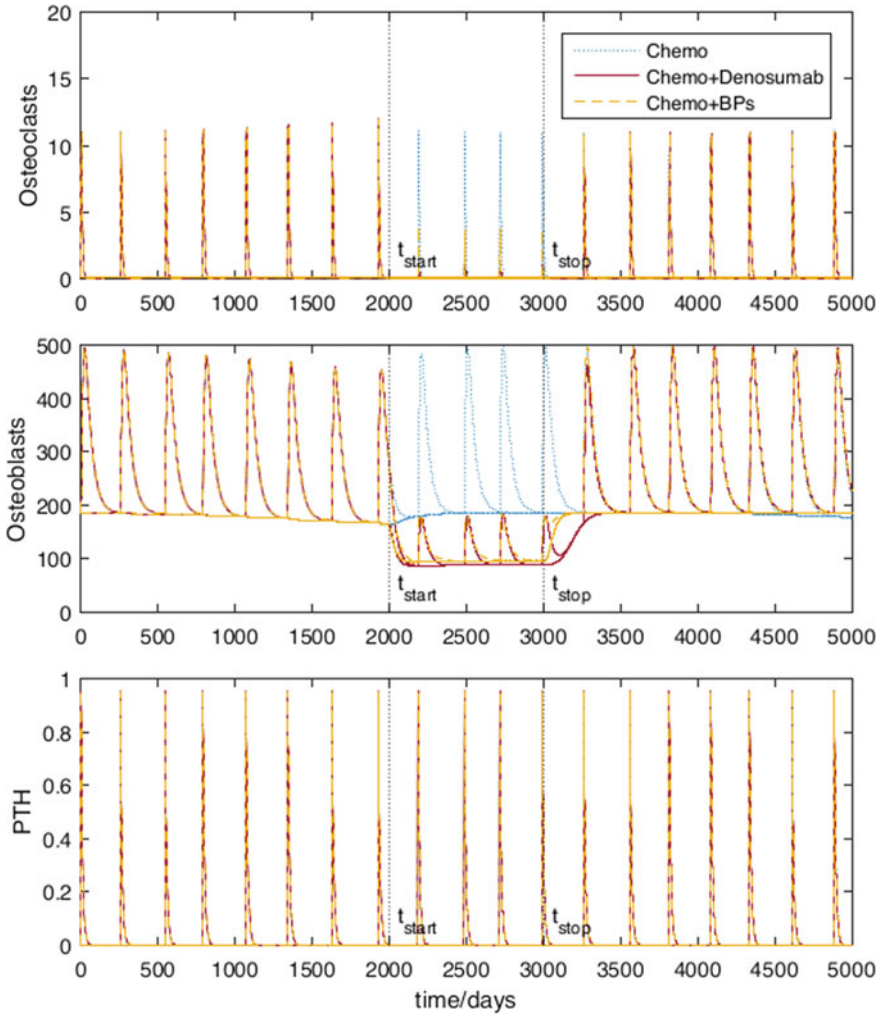

Fig. 5 Dynamics of bone microenvironment affected by metastases, with treatment through chemotherapy alone, chemotherapy combined with denosumab and combined with bisphosphonates, starting at time $t_{\text{start}} = 2000$ days and interrupted at $t_{\text{stop}} = 3000$ days. Following Eqs. (15a), (7b), (7c), (7d), (15b), (15c), and (7g), using the parameters from column *B* in Table 3, in accordance with [9]

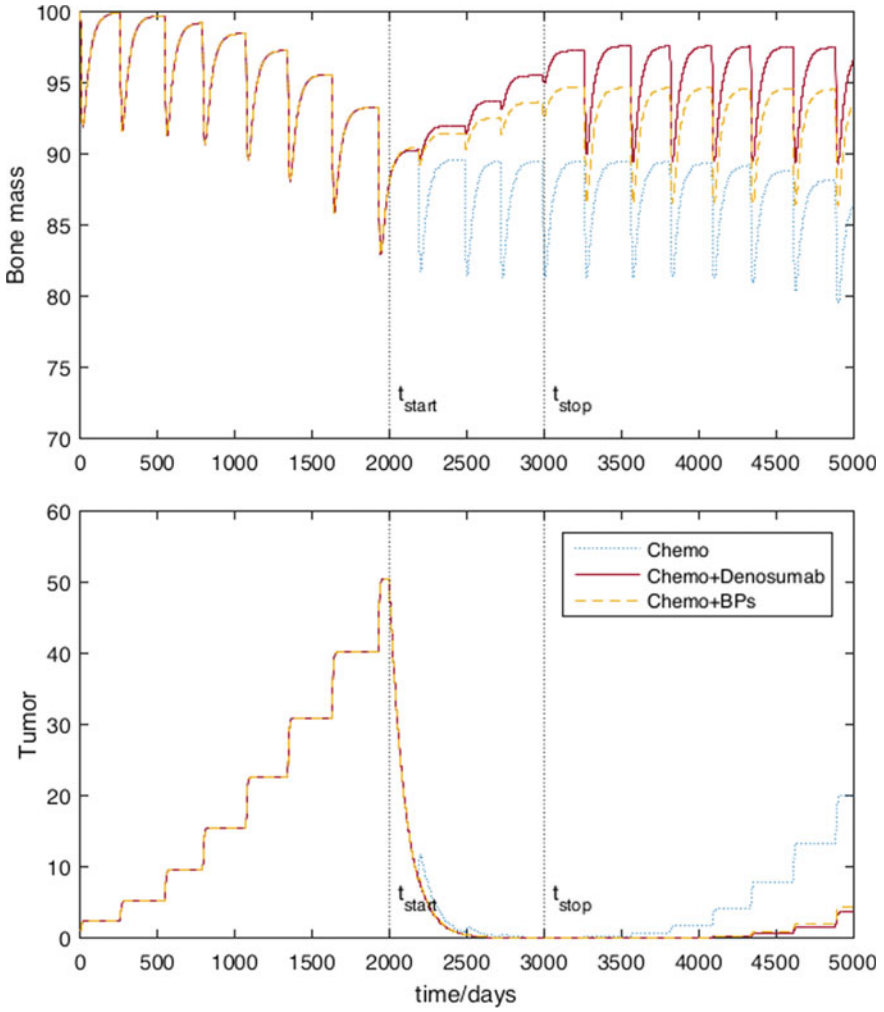

Fig. 6 Bone metastases and bone mass evolution, with treatment through chemotherapy alone, chemotherapy combined with denosumab and combined with bisphosphonates, starting at time $t_{start} = 2000$ days and interrupted at $t_{stop} = 3000$ days. Following Eqs. (15a), (7b), (7c), (7d), (15b), (15c), and (7g), using the parameters from column *B* in Table 3, in accordance with [9]

As it can be observed, the treatment with chemotherapy reduces the size of the tumor, but does not reduce bone loss during treatment. However, in combination with anti-resorptive therapy, it is possible to recover bone mass while eliminating tumor.

Table 3 Variables, parameters, and initial conditions of the simulated models: (*A*) Eqs. (1a)–(1c) [17], (*B*) Eqs. (15a), (7b), (7c), (7d), (15b), (15c), and (7g) [9], (*C*) Eqs. # [8]

Operator	Description				
D^1	First-order derivative, i.e., D^α with $\alpha = 1$				
D^α	Fractional order derivative				
$D^{\alpha(t)}$	Variable order derivative				
∇^2	Non-local, second-order, vector differential operator				
$\frac{\partial^2}{\partial x^2}$	Partial, second-order derivative for bone distance x				
Variable	Description	Units			
t	Time	day			
x	Adimensional distance along the bone	–			
$C(t, x)$	Number of osteoclasts	cells			
$B(t, x)$	Number of osteoblasts	cells			
$\text{PTH}_{\text{pool}}(t, x)$	PTH and PTHrP concentration variation	ng/L			
$T(t, x)$	Bone metastases size	%			
$z(t, x)$	Bone mass	%			
$d_1(t)$	Effect of denosumab	–			
$d_2(t)$	Effect of bisphosphonates	–			
$d_3(t)$	Effect of anti-cancer therapy	–			
$C_{th}(t, x)$	Threshold for active osteoclasts	cells			
$B_{th}(t, x)$	Threshold for active osteoblasts	cells			
$\alpha(t)$	Variable order for differential equations	cells			
Parameter	Description	Units	*Values A*	*Values B*	*Values C*
α	Fractional order of the equations	–	–	–	$\in]0, 2[$
σ_C	Diffusion coefficient of osteoclasts	–	–	–	10^{-6}
σ_B	Diffusion coefficient of osteoblasts	–	–	–	10^{-6}

(continued)

Table 3 (continued)

Parameter	Description	Units	*Values A*	*Values B*	*Values C*
σ_z	Diffusion coefficient of the bone	–	–	–	10^{-6}
σ_T	Diffusion coefficient of the tumor	–	–	–	10^{-6}
α_C	Osteoclasts activation rate	$\text{cell}^{-1}\ \text{day}^{-\alpha}$	3	3	3
α_B	Osteoblasts activation rate	$\text{cell}^{-1}\ \text{day}^{-\alpha}$	4	4	4
β_C	Osteoclasts apoptosis (programmed cell death) rate	$\text{day}^{-\alpha}$	0.2	0.2	0.2
β_B	Osteoblasts apoptosis rate	$\text{day}^{-\alpha}$	0.02	0.02	0.02
g_{CC}	Osteoclasts autocrine regulator	–	0.5	0.1	1.1
g_{BC}	Osteoblasts-derived osteoclasts paracrine regulator	–	−0.5	−1	−0.5
g_{CB}	Osteoclasts-derived osteoblasts paracrine regulator	–	1.0	0.8	1
g_{BB}	Osteoblasts autocrine regulator	–	0	0.2	0
k_C	Bone resorption rate	$\%\ \text{cell}^{-1}\ \text{day}^{-\alpha}$	0.24	0.5	0.45
k_B	Bone formation rate	$\%\ \text{cell}^{-1}\ \text{day}^{-\alpha}$	0.0017	0.00248723	0.0048
K_{PTH}	PTH growth rate	$\text{ng L}^{-1}\ \text{day}^{-\alpha}$	–	1	–
β_{PTH}	PTH and PTHrP degradation rate	$\text{day}^{-\alpha}$	–	0.1	–

(continued)

Table 3 (continued)

Parameter	Description	Units	*Values A*	*Values B*	*Values C*
$K_{\mathrm{PTH}_{\mathrm{pool}_{BC}}}$	Influence of PTH/PTHrP in RANKL/OPG ratio	ng^{-1} L	–	1.261	–
k_W	Shape parameter of Weibull distribution	–	–	15	–
λ_W	Scale parameter of Weibull distribution	–	–	300	–
k_T or γ_T	Bone metastases growth rate through bone resorption	% cell^{-1} $\mathrm{day}^{-\alpha}$	–	1	0.004
λ_T	Half-saturation constant for bone metastases size	%	–	10	–
L_T	Maximum size of bone metastases	%	–	100	100
r_{CC}	Effect of tumor in osteoclasts autocrine regulator	–	–	0.022	0.005
r_{CB}	Effect of tumor in osteoblasts-derived osteoclasts paracrine regulator	–	–	–	0
r_{BC}	Effect of tumor in Osteoclasts-derived osteoblasts paracrine regulator	–	–	–	0

(continued)

Table 3 (continued)

Parameter	Description	Units	*Values A*	*Values B*	*Values C*
r_{BB}	Effect of tumor in osteoblasts autocrine regulator	–	–	−0.198	0.2
r_{PTHrP}	Rate of PTHrP production by cancer cells	ng L^{-1} cell^{-1} $\text{day}^{-\alpha}$	–	0.0043	–
K_{d_1}	Maximum effect of denosumab	–	–	0.48	0.1
K_{d_2}	Maximum effect of bisphosphonates	$\text{day}^{-\alpha}$	–	1.2	0.1
K_{d_3}	Maximum effect of anti-cancer therapy	% $\text{day}^{-\alpha}$	–	0.017	2.3
C_{ss}	Steady-state value of $C(t, x)$	cells	1.06	–	
B_{ss}	Steady-state value of $B(t, x)$	cells	212.13	–	
Initial conditions	Description	Units	*Values A*	*Values B*	*Values C*
C_0 or $C(0, x)$	Initial number of osteoclasts	cells	$C_{ss} + 10$	C_{ss}	$C(0, x)$ [2]
B_0 or $B(0, x)$	Initial number of osteoblasts	cells	B_{ss}	B_{ss}	316
z_0 or $z(0, x)$	Initial bone mass percentage	%	100	100	100
$\text{PTH}_{\text{pool0}}$	Initial PTH and PTHrP concentration	ng/L	–	0	–
T_0 or $T(0, x)$	Initial size of bone metastases	%	–	1	

2.4 *Models Based on Fractional and Variable Order Derivatives*

2.4.1 Introduction to Fractional and Variable Order Calculus

Biological processes often present anomalous diffusion [21], and while it cannot be said with certainty that this is the case for bone remodeling, it is very likely that it be so. To account for this, it is necessary to introduce *fractional derivatives* in the existing mathematical models (such an adaptation has been done and studied in

[8]). Fractional derivatives are no more than a generalization of differentiation and integration of order $n \in \mathbb{N}$ to orders $\alpha \in \mathbb{R}$. The most natural and appealing example is that of the exponential function $f(x) = e^{ax}$, whose n*th* derivative is given simply by $a^n e^{ax}$. This suggests defining the derivative of order α that has not necessarily to be an integer, as $a^\alpha e^{ax}$. Since its idealization, the number of applications with fractional derivatives has been rapidly growing. Recently, the fractional order linear time invariant (FOLTI) systems have attracted significant attention in the control systems society [24], and fractional differential equations find a very wide range of applications: They are used to formulate and solve different physical models allowing a continuous transition from relaxation to oscillation phenomena; to predict the nonlinear survival and growth curves of foodborne pathogens; to adapt the viscoelasticity equations (Hooke's Law, Newtonian fluids Law), among other applications [34]. It also plays an important role in physics, thermodynamics, electrical circuits theory and fractances, mechatronics systems, signal processing, chemical mixing, chaos theory, to name a few [24]. However, many physical processes appear to exhibit a *fractional order behavior that varies with time or space*: In the field of viscoelasticity, the effect of temperature on the small amplitude creep behavior of certain materials is known to change its characteristics from elastic to viscoelastic or viscous, and real applications may require a time varying temperature to be analyzed; the relaxation processes and reaction kinetics of proteins that are described by fractional differential equations have been found to have a temperature dependence; the behavior of some diffusion processes in response to temperature changes can be better described using variable order elements rather than time varying coefficients; and more [20]. Such evidence allowed to consider that the fractional order of integrals and derivatives could be a function of time or some other variable, thus introducing the concept of variable order (or structure) operators, where the order of the operator is allowed to vary either as a function of the independent variable of integration or differentiation (t) or as a function of some other (perhaps spatial) variable (y) [20, 48]. More information on fractional and variable order calculus can be found in this chapter's Appendix.

2.4.2 Local Models with Variable Derivatives

A new model is proposed by the authors, where the model described in Eq. (6)— corresponding to local tumorous model, without treatment—was simplified by including variable order derivatives in the osteoclasts and osteoblasts equations, whose time-dependent order is given by $\alpha(t)$. Hence, by doing so, tumor itself would influence the order directly, and it is now the order responsible for the change in the behavior of the osteoclasts and osteoblasts, instead of inducing such behavior through the tumorous parameters (r_{ij}). The remaining parameters are to be set according to the healthy bone remodeling case, for periodic cycles.

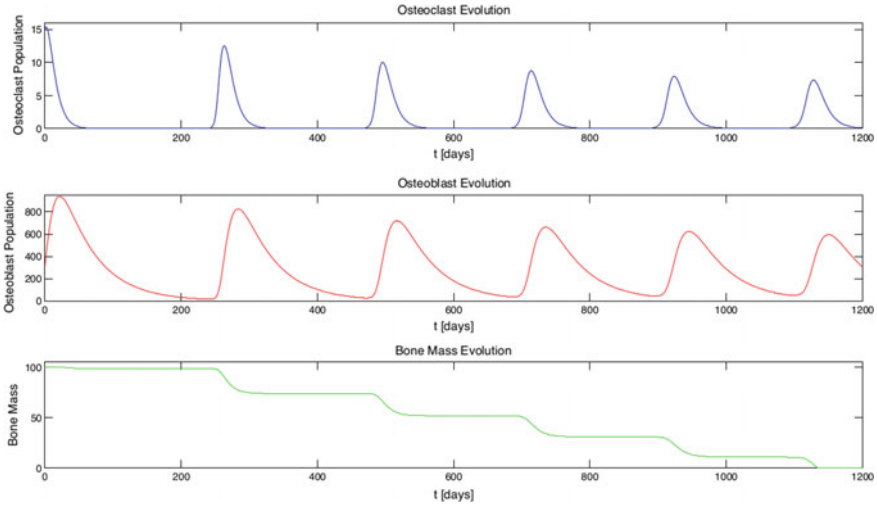

Fig. 7 Simulation results for the model in Sect. 2.4.2 simplifying the existing equations for the local tumorous influence in [2]. Parameters used for simulation are the same as the referred case

$$D^{\alpha(t)}C(t) = \alpha_C C(t)^{g_{CC}} B(t)^{g_{BC}} - \beta_C C(t) \tag{16a}$$

$$D^{\alpha(t)}B(t) = \alpha_B C(t)^{g_{CB}} B(t)^{g_{BB}} - \beta_B B(t) \tag{16b}$$

$$D^{1}T(t) = \gamma_T T(t) \log \frac{L_T}{T(t)} \tag{16c}$$

$$\alpha(t) = 1 - T(t)\rho(t), \quad \text{where} \quad \rho(t) = \frac{0.00005}{T_{\text{simulation}}} t = 4.1667 \times 10^{-8} t \tag{16d}$$

Bone mass, like in previous cases, reflects the behavior of the osteoclasts and osteoblasts and is thus the same as that of the original model in [17]. This model consists, consequently, in Eqs. (16a)–(16d) and (1c).

The advantage of this model with variable order differential equations over all previous models is that the same phenomena are modeled with far less parameters (See Fig. 7).

3 Non-local Models

The previous section addressed local models for bone remodeling represented mostly by ordinary differential equations (ODEs). Under this framework, only the dynamic behavior of individual BMUs is taken into account. The present section extends these models to one-dimensional geometries, thus modeling diffusion processes in the bone. We will focus on the proposals based on partial differential equations (PDEs) although other approaches also exist, such as in [1] that uses hybrid cellular automata

to describe spatiotemporal bone remodeling, both healthy and in the presence of bone metastases, and even the effect of anti-RANKL and bisphosphonates therapy.

3.1 Healthy Bone Remodeling

Ayati and colleagues [2] extend the model in [17], adding the effect in the bone dynamics and allowing for diffusion over one dimension (i.e., a one-dimensional bone is assumed), by introducing diffusion terms $\sigma \frac{\partial^2}{\partial x^2}$ into the osteoclasts, osteoblasts, and bone mass equations. Consequently, variables C, B, and z now depend on x as well as on t.

$$D^1 C(t,x) = \sigma_C \frac{\mathrm{d}^2}{\mathrm{d}x^2} C(t,x) + \alpha_C C(t,x)^{g_{CC}} B(t,x)^{g_{BC}} - \beta_C C(t,x) \tag{17a}$$

$$D^1 B(t,x) = \sigma_B \frac{\mathrm{d}^2}{\mathrm{d}x^2} B(t,x) + \alpha_B C(t,x)^{g_{CB}} B(t,x)^{g_{BB}} - \beta_B B(t,x) \tag{17b}$$

$$\begin{aligned} D^1 z(t,x) = {} & \sigma_z \frac{\partial^2}{\partial x^2} z(t,x) - k_C \max\{0, C(t,x) - C_{th}(t,x)\} \\ & + k_B \max\{0, B(t,x) - B_{th}(t,x)\} \end{aligned} \tag{17c}$$

In Eq. (17c), the diffusion term of $z(t,x)$ represents the stochastic nature of bone dynamics, but not cells migration. More information about variables and parameters can be found in Table 3. Other proposal by Ryser and colleagues [37] explicitly introduces OPG and RANKL as separate variables and includes the spatial evolution of a single BMU. The model is described by Eq. (18), assuming $g_{BB} = 0$ and, since OPG, ϕ_O, RANKL and ϕ_R are modeled explicitly, $g_{BC} = 0$.

$$\begin{aligned} D^1 C(t,x) = {} & \alpha_C C(t,x)^{g_{CC}} - \beta_C C(t,x) + f_1 \frac{\phi_R(t,x)}{\lambda + \phi_R(t,x)} \theta(y_C(t,x)) C(t,x) \\ & - \zeta \nabla \cdot (y_C(t,x) \nabla \phi_R(t,x)), \end{aligned} \tag{18a}$$

$$D^1 B(t,x) = \alpha_B C(t,x)^{g_{CB}} - \beta_B B(t,x), \tag{18b}$$

$$\begin{aligned} D^1 \phi_R(t,x) = {} & \alpha_R y_{B,t_R} + f_R \Delta(\phi_R^{\epsilon}(t,x)) - f_B \frac{\phi_R(t,x)}{\lambda + \phi_R(t,x)} \theta(y_C(t,x)) C(t,x) \\ & - f_{RO} \phi_R(t,x) \phi_O(t,x), \end{aligned} \tag{18c}$$

$$D^1 \phi_O(t,x) = \alpha_O y_{B,t_O} + f_O \Delta(\phi_O^{\delta}(t,x)) - f_{RO} \phi_R(t,x) \phi_O(t,x), \tag{18d}$$

$$\begin{aligned} D^1 z(t,x) &= -k_C \max\{0, C(t,x) - C_{ss}\} + k_B \max\{0, B(t,x) - B_{ss}\} \\ &= -k_C y_C(t,x) + k_B y_B(t,x) \end{aligned} \tag{18e}$$

The activation of osteoclasts is now dependent on autocrine parameters and RANK/RANKL binding, encoded by the term $f_1 \frac{\phi_R}{\lambda + \phi_R} \theta(y_C) C$. RANK receptors saturation threshold is described by a Hill function, with half-saturation concentration λ, and θ is the Heaviside function (thus $\theta(y_C) = 1$ if the number of active osteoclasts y_C verifies

$y_C > 0$; otherwise, $\theta(y_C) = 0$). Osteoclasts movement follows RANKL gradient, as described by the term $\zeta \nabla \cdot (y_C \nabla \phi_R)$, at migration rate ζ. RANKL and OPG are produced by active osteoblasts, considering that after osteoblasts precursors become mature, there is a time delay t_R and t_O before they can produce RANKL and OPG, encoded by y_{B,t_R} and y_{B,t_O}, respectively. RANKL and OPG porous diffusion in the bone is given by $f_R \Delta(\phi_R^{\epsilon})$ and $f_O \Delta(\phi_O^{\delta})$, at rates f_R and f_O. The binding of OPG to RANKL is described by the term $f_{RO} \phi_R \phi_O$, which is present in both O and R dynamics. For RANKL, however, an additional term $f_2 \frac{\phi_R}{\lambda + \phi_R} \theta(y_C) C$ encodes the RANK/RANKL binding in osteoclasts precursors, at rate f_2, similarly to the term in (18a). Sensitivity analysis and parameter estimation are conducted for this model in [36]. The model of [27] is extended in [4] by adding spatial evolution to the different components of the model and by introducing appropriate fluxes in cells and regulatory agents. Fluxes represent transport processes, such as diffusion or chemotaxis. This model is able to capture the known organized structure of a BMU, presenting a resorption zone at the front, then a reversal zone and lastly a bone formation zone. The model also captures how PTH and the RANK/RANKL/OPG pathway affect the bone cells in the different stages of maturation and during bone remodeling.

3.2 Models Including the Tumor Burden

Ayati and colleagues [2] also extended the model proposed in [17] by including the diffusion process of multiple myeloma disease effects on bone dynamics:

$$D^1 C(t,x) = \sigma_C \frac{\partial^2}{\partial x^2} C(t,x) + \alpha_C C(t,x)^{g_{CC}\left(1 + r_{CC} \frac{T(t,x)}{L_T}\right)} B(t,x)^{g_{BC}\left(1 + r_{BC} \frac{T(t,x)}{L_T}\right)} - \beta_C C(t,x) \tag{19a}$$

$$D^1 B(t,x) = \sigma_B \frac{\partial^2}{\partial x^2} B(t,x) + \alpha_B C(t,x)^{\frac{g_{CB}}{1 + r_{CB} \frac{T(t,x)}{L_T}}} B(t,x)^{g_{BB} - r_{BB} \frac{T(t,x)}{L_T}} - \beta_B B(t,x) \tag{19b}$$

$$D^1 T(t,x) = \sigma_T \frac{\partial^2}{\partial x^2} T(t,x) + \gamma_T T(t,x) \log\left(\frac{T(t,x)}{L_T}\right) \tag{19c}$$

This model's bone mass equation is (17c). The tumorous variables and parameters now introduced have the same meaning as in the local case (see Sect. 2.2), except that $T(t)$ and $T(0)$ are now given by $T(t,x)$ and $T(0,x)$, respectively.

In [38], the effect of osteolytic bone metastases is included in the bone remodeling model in [36], accounting for spatial diffusion, as described by Eq. (20).

$$D^1 C(t,x) = \alpha_C C(t,x)^{g_{CC}} - \beta_C C(t,x) + f_1 \frac{\phi_R(t,x)}{\lambda + \phi_R(t,x)} y_C(t,x) - \zeta \frac{\partial}{\partial x}\left(y_C(t,x) \frac{\partial \phi_R(t,x)}{\partial x}\right), \tag{20a}$$

$$D^1\phi_R(t,x) = k_{_R}\phi_P(t,x)z(t) + \tau_R T(t,x) + f_R\frac{\partial^2\phi_R(t,x)}{\partial x^2} - f_{_B}\frac{\phi_R(t,x)}{\lambda+\phi_R(t,x)}y_C(t,x) - f_{RO}\phi_R(t,x)\phi_O(t,x), \quad (20b)$$

$$D^1\phi_O(t,x) = \tau_O T(t,x) + S_{_O} + f_{_O}\frac{\partial^2\phi_O(t,x)}{\partial x^2} - \beta_O\phi_O(t,x) - f_{RO}\phi_R(t,x)\phi_O(t,x), \quad (20c)$$

$$D^1\phi_P(t,x) = \tau_{_P}T(t,x) + f_{_P}\frac{\partial^2\phi_P(t,x)}{\partial x^2} - \beta_{_P}\phi_P(t,x), \quad (20d)$$

$$D^1 z(t,x) = -k_{_C}\max\{0, C(t,x) - C_{th}\} = -k_{_C}y_C(t,x), \quad (20e)$$

$$T(t,x) = 1 - z(t,x) \quad (20f)$$

This model assumes bone formation to be much slower than bone resorption and tumor growth in the presence of osteolytic bone metastases. As such, the osteoblast dynamics is not taken into account and is removed from the model. Hence, bone mass dynamics z in Eq. (20e) is dominated by bone resorption and tumor cells T fill in the space left in the bone after resorption. Tumor-derived PTHrP ϕ_P increases the production of RANKL ϕ_R by osteoblasts. Also, tumor cells can also produce RANKL. The conjugation of these factors leads to increased bone resorption in areas close to the tumor, which contributes to tumor growth, and thus the vicious cycle of bone metastases is captured by this model.

3.3 Non-local Treatment Approach

3.3.1 Normal Cell Diffusion

Following what was done in [2], a treatment possibility is applied accounting for the effects of proteasome inhibition ($V_1(t)$) and anti-cancer therapy ($V_2(t)$) in myeloma bone disease, similarly to what was done locally in the model (14). For the following equation, when $t < t_{\text{start}}$, treatment is yet to be started.

$$V_1(t) = \upsilon_1, \quad \text{for } t \geq t_{\text{start}} \quad (21a)$$

$$V_2(t) = \upsilon_2, \quad \text{for } t \geq t_{\text{start}} \quad (21b)$$

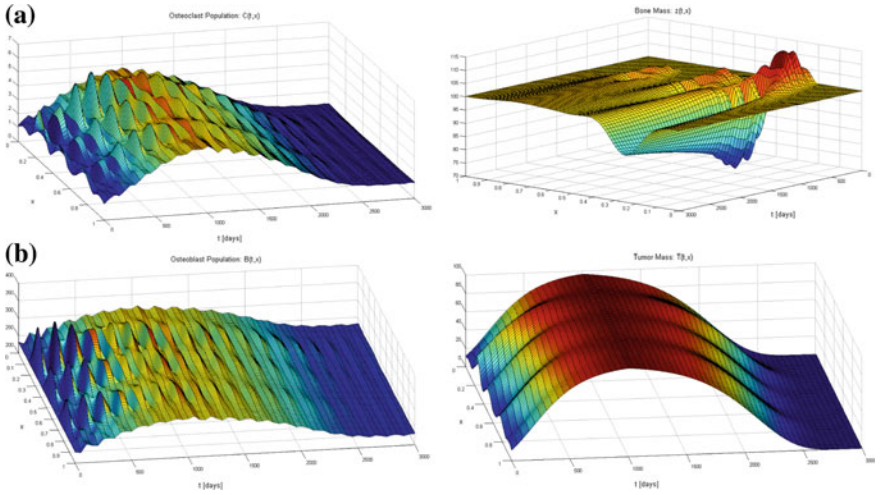

Fig. 8 Bone model simulation with an initial distribution of osteoclasts and tumor by $C(0, x) = T(0, x)$, as $C(0, x)$ presented in [2], where **a** represents the osteoclast evolution, and **b** the osteoblast evolution. Treatment was introduced at $t_{\text{start}} = 1000$ days, with parameters $V_1(t) = \upsilon_1 = 0.0005$ and $V_2(t) = \upsilon_2 = 0.007$. Non-spatial and bone mass parameters were set according to the local model presented for periodic remodeling cycles (see column A of Table 3) and as in the one-dimensional model without tumor (see [2] for more details), respectively; and all of the tumor-related parameters are the same as in the local case

$$D^1 C(t,x) = \sigma_C \frac{\partial^2}{\partial x^2} C(t,x) + \alpha_C C(t,x)^{g_{CC}\left(1+r_{CC}\frac{T(t,x)}{L_T}\right)} B(t,x)^{g_{BC}\left(1+r_{BC}\frac{T(t,x)}{L_T}\right)} - \beta_C C(t,x) \tag{22a}$$

$$D^1 B(t,x) = \sigma_B \frac{\partial^2}{\partial x^2} B(t,x) + \alpha_B C(t,x)^{\left(\frac{g_{CB}}{1+r_{CB}\frac{T(t,x)}{L_T}}\right)} B(t,x)^{\left(g_{BB}-r_{BB}\frac{T(t,x)}{L_T}\right)} - \left(\beta_B - V_1(t)\right) B(t,x) \tag{22b}$$

$$D^1 T(t,x) = \sigma_T \frac{\partial^2}{\partial x^2} T(t,x) + \left(\gamma_T - V_2(t)\right) T(t,x) \log\left(\frac{T(t,x)}{L_T}\right) \tag{22c}$$

Again, the bone mass equation is (17c) (non-local healthy bone remodeling case). Simulations for such treatment, and its effect on the bone microenvironment, can be seen in Fig. 8, where the tumor is of initial small intensity, acting in several areas of the spatial bone environment x, but growing over time. Bone resorption and formation, both temporal and spatially, are disrupted with a delayed response from the osteoblast population [2]. Consequently, an increased bone mass loss is observed in areas where the tumor has a more intense effect until treatment is introduced at $t_{\text{start}} = 1000$ days. Osteoclast production is then promoted, and the tumor growth inhibited until its significant reduction and regular bone dynamics coupling are achieved. Bone mass

only partially recovers, since areas of the bone where the tumor effect was stronger were unable to fully recover its original density.

The pharmacokinetics and pharmacodynamics presented in Sect. 2.3.1 can also be integrated with non-local bone remodeling models. This was done in [8], by considering that each drug's pharmacodynamic effect to be the same throughout the bone, for the same time instance. Again, the effect of a drug, $d_i(t)$, is given by Eq. (13), where $d_1(t)$ is the effect of bisphosphonates; $d_2(t)$ represents denosumab; and chemotherapy is encompassed in $d_{34}(t)$ (it is noted that, in [8], chemotherapy is considered to be a combination of two distinct drugs, hence the subscript 34). Simulation results, from [8], can be found in Fig. 9. This model's bone mass equation is once more (17c) (non-local healthy bone remodeling case), and the remaining equations are as follows.

$$\begin{aligned} D^1 C(t,x) &= \sigma_C \frac{\partial^2}{\partial x^2} C(t,x) \\ &\quad + \alpha_C C(t,x)^{g_{CC}\left(1+r_{CC}\frac{T(t,x)}{L_T}\right)} B(t,x)^{g_{BC}\left(1+r_{BC}\frac{T(t,x)}{L_T}\right)\left(1+K_{d_1}d_1(t)\right)} \\ &\quad - \left(1+K_{d_2}d_2(t)\right)\beta_C C(t,x) \end{aligned} \tag{23a}$$

$$\begin{aligned} D^1 B(t,x) &= \sigma_B \frac{\partial^2}{\partial x^2} B(t,x) + \alpha_B C(t,x)^{\left(\frac{g_{CB}}{1+r_{CB}\frac{T(t,x)}{L_T}}\right)} B(t,x)^{\left(g_{BB}-r_{BB}\frac{T(t,x)}{L_T}\right)} \\ &\quad - \beta_B B(t,x) \end{aligned} \tag{23b}$$

$$D^1 T(t,x) = \sigma_T \frac{\partial^2}{\partial x^2} T(t,x)$$

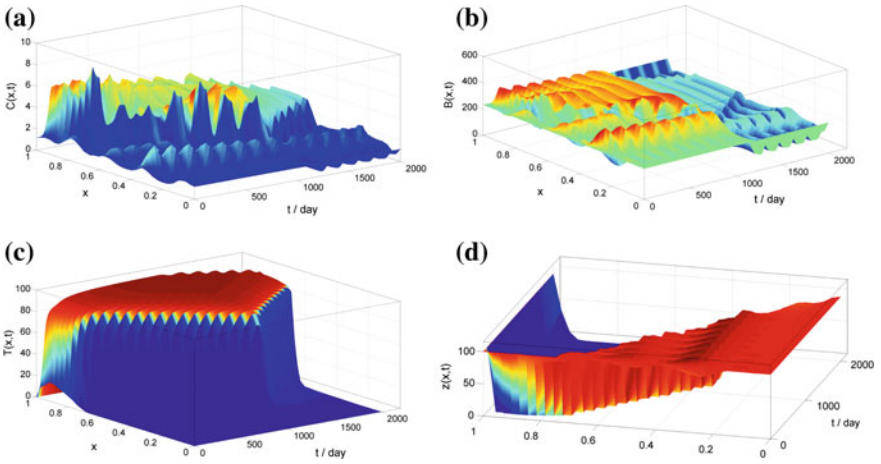

Fig. 9 Simulation of model of Eq. 23, where **a** is the osteoclasts evolution, **b** the osteoblasts evolution, **c** the tumorous influence, and **d** the consequences for the bone mass. Used parameters can be found in column *C* of Table 3

$$+\left(1-K_{d_{34}}d_{34}(t)\right)\gamma_T T(t,x)^a\left(\frac{T(t,x)}{L_T}\right)^b \tag{23c}$$

Although different set of parameters were used, when compared to the local model in Eq. 15 and considering the different used expressions for the tumor evolution, the results behave similarly. The tumor is extinguished as osteoclasts and osteoblasts recover their steady-state value.

3.3.2 Working with Fractional Derivatives

Anomalous diffusion corresponds to partial differential equations with fractional derivatives in order to time and second-order derivatives in order to space [21]. In what pharmacokinetic and pharmacodynamic models are concerned, those presented in Sect. 2.3.1 were achieved for models with integer orders derivatives. Hence, they cannot be directly applied when one is considering fractional order: New PK equations are introduced and assumed to have the same fractional order as the model itself. Such adaptation is given by Eq. (24), where α is the fractional order of the system. The PD component, however, remains as in Eq. (13).

$$D^\alpha C_g(t) = -k_a C_g(t) \tag{24a}$$

$$D^\alpha C_p(t) = k_a C_g(t) - k_e C_p(t) \tag{24b}$$

$$C_P^0 = \frac{D_0 F}{V_d} \tag{24c}$$

$$d(t) = \frac{C_p(t)}{C_{50} + C_p(t)} \tag{24d}$$

The model from Eq. (23) is, but, a particular case of a general anomalous diffusion case, corresponding to setting the describing fractional order to $\alpha = 1$. The general model of order α (including for the PK/PD treatment) is as follows [8].

$$\begin{aligned} D^\alpha C(t,x) = {} & \sigma_c \frac{\partial^2}{\partial x^2} C(t,x) \\ & + \alpha_c C(t,x)^{g_{CC}\left(1+r_{CC}\frac{T(t,x)}{L_T}\right)} B(t,x)^{g_{BC}\left(1+r_{BC}\frac{T(t,x)}{L_T}\right)\left(1+K_{d_1}d_1(t)\right)} \\ & - \left(1+K_{d_2}d_2(t)\right)\beta_c C(t,x) \end{aligned} \tag{25a}$$

$$\begin{aligned} D^\alpha B(t,x) = {} & \sigma_B \frac{\partial^2}{\partial x^2} B(t,x) + \alpha_B C(t,x)^{\left(\frac{g_{CB}}{1+r_{CB}\frac{T(t,x)}{L_T}}\right)} B(t,x)^{\left(g_{BB}-r_{BB}\frac{T(t,x)}{L_T}\right)} \\ & - \beta_B B(t,x) \end{aligned} \tag{25b}$$

$$\begin{aligned} D^\alpha z(t,x) = {} & \sigma_z \frac{\partial^2}{\partial x^2} z(t,x) - k_c \max\{0, C(t,x) - C_{th}(t,x)\} \\ & + k_B \max\{0, B(t,x) - B_{th}(t,x)\} \end{aligned} \tag{25c}$$

$$D^{\alpha}T(t,x) = \sigma_T \frac{\partial^2}{\partial x^2} T(t,x) + \left(1 - K_{d_{34}} d_{34}(t)\right) \gamma_T T(t,x)^a \left(\frac{T(t,x)}{L_T}\right)^b \tag{25d}$$

Also, the local PTH model in Eq. (15) was extended to a three-dimensional case in [45]. This was done replacing variable $\chi(t,x)$ (where χ can be C, B, T, z, C_{th} or B_{th}) with $\chi(t,\mathbf{x}) = \chi(t,x_1,x_2,x_3)$ and using the Laplacian operator $\nabla = \frac{\partial^2}{\partial x_1^2} + \frac{\partial^2}{\partial x_2^2} + \frac{\partial^2}{\partial x_3^2}$ instead of $\frac{\partial^2}{\partial x^2}$. However, for comparison sake, only the one-dimensional version is presented next.

$$D^{\alpha}C(t,x) = \sigma_C \frac{\partial^2}{\partial x^2} C(t,x) + \alpha_C C(t,x)^{g_{CC} + r_C \frac{T(t,x)}{L_T}} B(t,x)^{g_{BC} + K_{\text{PTH}_{\text{pool}21}} \text{PTHpool}(t,x) - K_{d_1} d_1(t)} - (\beta_B + K_{d_2} d_2(t)) C(t,x) \tag{26a}$$

$$D^{\alpha}B(t,x) = \sigma_B \frac{\partial^2}{\partial x^2} B(t,x) + \alpha_B C(t,x)^{g_{CB}} B(t,x)^{g_{BB} + r_B \frac{T(t,x)}{L_T}} - \beta_B B(t,x) \tag{26b}$$

$$D^{\alpha}\text{PTH}_{\text{pool}}(t,x) = -\beta_{\text{PTH}} \text{PTH}_{\text{pool}}(t,x) + K_{\text{PTH}} \delta(t) + r_{\text{PTHrP}} \max\{0, C(t,x) - C_{th}(t,x)\} \frac{T(t,x)}{L_T} \tag{26c}$$

$$P(\delta(t) = 1) = 1 - e^{-\left(\frac{t}{\lambda_W}\right)^{k_W}} \tag{26d}$$

$$D^{\alpha}T(t,x) = \sigma_T \frac{\partial^2}{\partial x^2} T(t,x) + k_T \max\{0, C(t,x) - C_{th}(t,x)\} \frac{T(t,x)}{\lambda_T + T(t,x)} - K_{d_3} d_3(t) T(t,x) \tag{26e}$$

$$D^{\alpha}C_{th}(t,x) = \alpha_C C_{th}(t,x)^{g_{CC} + r_C \frac{T(t,x)}{L_T}} B_{th}(t,x)^{g_{BC} - K_{d_1} d_1(t)} - (\beta_C + K_{d_2} d_2(t)) C_{th}(t,x) \tag{26f}$$

$$D^{\alpha}B_{th}(t,x) = \alpha_B C_{th}(t,x)^{g_{CB}} B_{th}(t,x)^{g_{BB} + r_B \frac{T(t,x)}{L_T}} - \beta_B B_{th}(t,x) \tag{26g}$$

The bone mass equation of this model is in Eq. (25c) for an order α. Simulations of this model can be found in Fig. 10.

Table 3 lists variables and parameters, used throughout presented simulations, giving their meaning and dimensions.

4 Conclusions and Future Work

This chapter overviewed some of the most recent models for bone remodeling dynamics that take into account the biochemical microenvironment and the main cellular

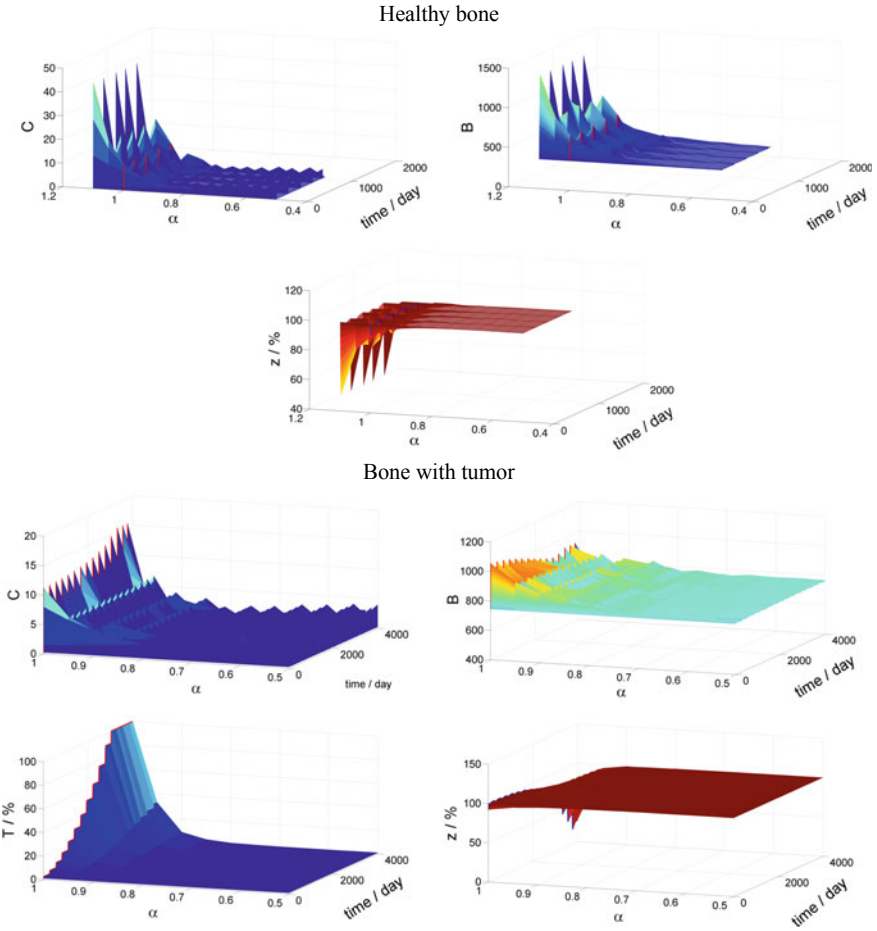

Fig. 10 Equation (26) model simulation, comparing the effect of several values of α on the model dynamics, where the $\alpha = 1$ case is represented by either a blue or red line. On the **left**, a healthy bone environment is represented and, on the **right**, a tumorous bone environment. From [45]

processes. These computational models allow for the integration of pathological phenomena such as cancer and also accommodate pharmacokinetic/pharmacodynamic (PK/PD) information.

There are many other models for the bone that are focused on the biomechanical aspects of the system, addressed in other chapters of this book. As future work, it would be crucial to integrate both approaches, as to improve the models in terms of accuracy to describe the real organ. In fact, these parallel lines of research are already being integrated in recent years. Scheiner, Pivonka, and colleagues [25, 42] proposed models that include the coupled regulations of geometrical, biomechanical, and biochemical factors. The ODE system uses biochemical factors already addressed

such as TGFβ, RANK and RANKL, OPG and PTH with the f_{vas}, S_v and Ψ_{bm} of BMU. Although very complete, this model does not take into account one entire bone (e.g., femur) and the corresponding spatial effects, neither the inclusion of input functions representing PK/PD of the therapeutic drugs. These therapies were also analyzed separately, such as denosumab and bisphosphonates for osteoporosis [11, 41]. It is expected that all of these modeling and computational analysis of bone physiology will have an impact on the development of clinical decision support systems in the future.

Acknowledgements This work was supported by FCT, through IDMEC, under LAETA, projects UID/EMS/50022/2019 and BoneSys (Bone biochemical and biomechanic integrated modeling: addressing remodeling, disease and therapy dynamics), joint Polish–Portuguese project "Modeling and controlling cancer evolution using fractional calculus", and PERSEIDS (PTDC/EMS-SIS/0642/2014). R. Moura Coelho acknowledges the support by grant ZEUGMA-BiNOVA, number AD0075. S. Vinga acknowledges the support by Program Investigador FCT (IF/00653/2012) from FCT, co-funded by the European Social Fund (ESF) through the Operational Program Human Potential (POPH).

Appendix: Fractional and Variable Order Derivatives

To formally define fractional derivatives (*fractional* is the historical name, though order α can be irrational or have an imaginary part), one can present the Grünwald–Letnikoff construction, usually denoted by $D^{\alpha} f(t)$. The upper limit of the summations was set so that D^{-k}, $k \in \mathbb{N}$ to retrieve Riemann integrals: ${}_cD_t^{-1} f(t) = \int_c^t f(t)\,\mathrm{d}t$, and in general

$$ {}_cD_t^{-k} f(t) = \underbrace{\int_c^t \ldots \int_c^t f(t)\,\mathrm{d}t \ldots \mathrm{d}t}_{k \text{ integrations}}, \; k \in \mathbb{N} \tag{27} $$

Since it is not always reasonable to call c and t limits of integration, they are usually called terminals instead.

The Grünwald–Letnikoff construction is as follows.

$$ {}_cD_t^{\alpha} f(t) = \lim_{h \to 0^+} \frac{\sum_{k=0}^{[\frac{t-c}{h}]} (-1)^k \binom{a}{k} f(t - kh)}{h^{\alpha}} \tag{28} $$

where $\binom{a}{k}$ are the combinations of a things k at a time, given by

$$\binom{a}{k} = \begin{cases} \frac{\Gamma(\alpha+1)}{\Gamma(k+1)\Gamma(\alpha-k+1)}, & \text{if } \alpha, k, (\alpha-k) \in \mathbb{R} \setminus \mathbb{Z}^- \\ \frac{(-1)^k \Gamma(k-\alpha)}{\Gamma(k+1)\Gamma(-\alpha)}, & \text{if } \alpha \in \mathbb{Z}^- \wedge k \in \mathbb{Z}_0^+ \\ 0, & \text{if } (k \in \mathbb{Z}^- \vee (k-\alpha) \in \mathbb{N}) \wedge \alpha \notin \mathbb{Z}^- \end{cases} \tag{29}$$

Function $\Gamma(z),\ z \in \mathbb{C} \setminus \mathbb{Z}_0^-$ generalizes the factorial since $\Gamma(k+1) = k!,\ k \in \mathbb{Z}_0^+$.

Since α can assume any real value, it is possible to make it change with time (continuously or not). There are different reasonable ways of accounting for a time varying order $\alpha(t)$, again considering the Grünwald–Letnikoff definition. The two most straightforward options are given below:

- in the first, the argument of the order is simply the current value of t, meaning that the result at a given instant will not depend on previous values of the order $\alpha(t)$:

$${}_cD_t^{\alpha(t)} f(t) = \lim_{h \to 0^+} \frac{\sum_{k=0}^{\left|\frac{t-c}{h}\right|} (-1)^k \binom{\alpha(t)}{k} f(t-kh)}{h^{\alpha(t)}} \tag{30}$$

- in the second, the argument of α in the summation is the same argument of f, leading to a memory of previous values of the order [48]:

$${}_cD_t^{\alpha(t)} f(t) = \lim_{h \to 0^+} \sum_{\boldsymbol{k=0}}^{\left|\frac{t-c}{h}\right|} \frac{(-1)^k \binom{\boldsymbol{\alpha(t-kh)}}{k} f(t-kh)}{h^{\boldsymbol{\alpha(t-kh)}}} \tag{31}$$

Other possible definitions exist [43, 47]. Since it is reasonable to expect the previous evolution of a metastasis to have influence in the present time, variable order models presented presume this type of definition.

Readers interested in details can consult [21, 23, 39, 46, 48], which also address alternative definitions of fractional derivatives (namely those of Riemann–Liouville and of Caputo, that will, for functions well-behaved enough, lead to similar results).

Letting h have a small but finite value, approximations of fractional derivatives can be obtained. Values can be stored in matrices updated iteratively. This is the idea behind the numerical method of [29, 31, 32], termed matrix approach to discrete fractional calculus, used for the simulations in this chapter through MATLAB toolbox [30].

References

1. Araujo A, Cook LM, Lynch CC, Basanta D (2014) An integrated computational model of the bone microenvironment in bone-metastatic prostate cancer. Cancer Res 74(9):2391–401
2. Ayati BP, Edwards CM, Webb GF, Wikswo JP (2010) A mathematical model of bone remodeling dynamics for normal bone cell populations and myeloma bone disease. Biol Direct 5:28
3. Bellido T, Plotkin LI, Bruzzaniti A (2014) Bone Cells (Chap. 2). In: Basic and applied bone biology. Academic Press, Cambridge, pp 27 – 45

4. Buenzli PR, Pivonka P, Smith DW (2011) Spatio-temporal structure of cell distribution in cortical bone multicellular units: a mathematical model. Bone 48(4):918–26
5. Casimiro S, Ferreira AR, Mansinho A, Alho I, Costa L (2016) Molecular mechanisms of bone metastasis: which targets came from the bench to the bedside? Int J Mol Sci 17(9):1415
6. Casimiro S, Guise TA, Chirgwin J (2009) The critical role of the bone microenvironment in cancer metastases. Mol Cell Endocrinol 310(1–2):71–81
7. Chen Y-C, Sosnoski DM, Mastro AM (2010) Breast cancer metastasis to the bone: mechanisms of bone loss. Breast Cancer Res: BCR 12(6):215
8. Christ LF, Valério D, Coelho R, Vinga S (2018) Models of bone metastases and therapy using fractional derivatives. J Appl Nonlinear Dyn 7(1):81–94
9. Coelho RM, Lemos JM, Valério D, Alho I, Ferreira AR, Costa L, Vinga S (2016) Dynamic modeling of bone metastasis, microenvironment and therapy–integrating parathyroid hormone (PTH) effect, antiresorptive treatment and chemotherapy. J Theor Biol 391:1–12
10. Crockett JC, Rogers MJ, Coxon FP, Hocking LJ, Helfrich MH (2011) Bone remodelling at a glance. J Cell Sci 124(Pt 7):991–8
11. Cummings SR, San Martin J, McClung MR, Siris ES, Eastell R, Reid IR, Delmas P, Zoog HB, Austin M, Wang A, Kutilek S, Adami S, Zanchetta J, Libanati C, Siddhanti S, Christiansen C, Trial FREEDOM (2009) Denosumab for prevention of fractures in postmenopausal women with osteoporosis. New England J Med 361(8):756–765
12. Dhillon S, Kostrzewski A (2006) Basic pharmacokinetics (Chap. 1). In: Clinical pharmacokinetics, 1 edn. Pharmaceutical Press (2006)
13. Graham JM, Ayati BP, Holstein SA, Martin JA (2013) The role of osteocytes in targeted bone remodeling: a mathematical model. PloS one 8(5):10–14
14. Guise TA, Mundy GR (1998) Cancer and bone. Endocr Rev 19(1):18–54
15. Hood L, Friend SH (2011) Predictive, personalized, preventive, participatory (P4) cancer medicine. Nat Rev Clin Oncol 8(3):184–187
16. Komarova SV (2005) Mathematical model of paracrine interactions between osteoclasts and osteoblasts predicts anabolic action of parathyroid hormone on bone. Endocrinology 146(8):3589–95
17. Komarova SV, Smith RJ, Dixon SJ, Sims SM, Wahl LM (2003) Mathematical model predicts a critical role for osteoclast autocrine regulation in the control of bone remodeling. Bone 33(2):206–215
18. Lemaire V, Tobin FL, Greller LD, Cho CR, Suva LJ (2004) Modeling the interactions between osteoblast and osteoclast activities in bone remodeling. J Theor Biol 229(3):293–309
19. Liò P, Paoletti N, Moni MA, Atwell K, Merelli E, Viceconti M (2012) Modelling osteomyelitis. BMC Bioinf 13(Suppl 14):S12
20. Lorenzo CF, Hartley TT (2002) Variable order and distributed order fractional operators. Technical Report National Aeronautics and Space Administration (NASA)
21. Magin RL (2004) Fractional Calculus in Bioengineering. Begell House
22. Makatsoris T, Kalofonos HP (2009) The role of chemotherapy in the treatment of bone metastases. In: Kardamakis D, Vassiliou V, Chow E (eds) Bone metastases, volume 12 of Cancer metastasis biology and treatment. Springer Netherlands, Dordrecht, pp 287–297
23. Miller KS, Ross B (1993) An introduction to the fractional calculus and fractional differential equations. Wiley, New York
24. Petrás I (2009) Stability of fractional-order systems with rational orders: a survey. Int J Theory Appl 12(3)
25. Pivonka P, Buenzli PR, Scheiner S, Hellmich C, Dunstan CR (2013) The influence of bone surface availability in bone remodelling-a mathematical model including coupled geometrical and biomechanical regulations of bone cells. Eng Struct 47:134–147
26. Pivonka P, Komarova SV (2010) Mathematical modeling in bone biology: from intracellular signaling to tissue mechanics. Bone 47(2):181–189
27. Pivonka P, Zimak J, Smith DW, Gardiner BS, Dunstan CR, Sims NA, Martin TJ, Mundy GR (2008) Model structure and control of bone remodeling: a theoretical study. Bone 43(2):249–63

28. Pivonka P, Zimak J, Smith DW, Gardiner BS, Dunstan CR, Sims NA, Martin TJ, Mundy GR (2010) Theoretical investigation of the role of the RANK-RANKL-OPG system in bone remodeling. J Theor Biol 262(2):306–16
29. Podlubny I (2000) Matrix approach to discrete fractional calculus. Fractional Calc Appl Anal 3(4):359–386
30. Podlubny I (2012) Matrix approach to distributed-order ODEs and PDEs. http://www.mathworks.com/matlabcentral/fileexchange/36570-matrix-approach-to-distributed-order-odes-and-pdes
31. Podlubny I, Chechkin A, Skovranek T, Chen YQ, Jara BMV (2009) Matrix approach to discrete fractional calculus II: partial fractional differential equations. J Comput Phys 228:3137–3153
32. Podlubny I, Skovranek T, Jara BMV, Petras I, Verbitsky V, Chen YQ (1990) Matrix approach to discrete fractional calculus III: non-equidistant grids, variable step length and distributed orders. Philos Trans R Soc A 371:2013
33. Raggatt LJ, Partridge NC (2010) Cellular and molecular mechanisms of bone remodeling. J Biol Chem 285(33):25103–8
34. Rahimy M (2010) Applications of fractional differential equations. Appl Math Sci 4(50):2453–2461
35. Roodman GD (2004) Mechanisms of bone metastasis. New England J Med 360(16):1655–1664
36. Ryser MD, Komarova SV, Nigam N (2010) The cellular dynamics of bone remodeling: a mathematical model. SIAM J Appl Math 70(6):1899–1921
37. Ryser MD, Nigam N, Komarova SV (2009) Mathematical modeling of spatio-temporal dynamics of a single bone multicellular unit. J Bone Mineral Res 24(5):860–70
38. Ryser MD, Qu Y, Komarova SV (2012) Osteoprotegerin in bone metastases: mathematical solution to the puzzle. PLoS Comput Biol 8(10):e1002703
39. Samko SG, Kilbas AA, Marichev OI (1993) Fractional integrals and derivatives. Gordon and Breach, Yverdon
40. Savageau MA (1988) Introduction to S-systems and the underlying power-law formalism. Math Comput Modell 11:546–551
41. Scheiner S, Pivonka P, Smith DW, Dunstan CR, Hellmich C (2014) Mathematical modeling of postmenopausal osteoporosis and its treatment by the anti-catabolic drug denosumab. Int J Numer Methods Biomed Eng 30(1):1–27
42. Scheiner S, Pivonka P, Hellmich C (2013) Coupling systems biology with multiscale mechanics, for computer simulations of bone remodeling. Comput Methods Appl Mech Eng 254:181–196
43. Sierociuk D, Malesza W, Macias M (2016) Numerical schemes for initialized constant and variable fractional-order derivatives: matrix approach and its analog verification. J Vib Control 22(8):2032–2044
44. Suva LJ, Washam C, Nicholas RW, Griffin RJ (2011) Bone metastasis: mechanisms and therapeutic opportunities. Nat Rev Endocrinol 7(4):208–18
45. Valério D, Coelho R, Vinga S (2016) Fractional dynamic modelling of bone metastasis, microenvironment and therapy. In: International conference on fractional differentiation and its applications
46. Valério D, da Costa JS (2011) Introduction to single-input, single-output Fractional Control. IET Control Theor Appl 5(8):1033–1057
47. Valério D, da Costa JS (2011) Variable-order fractional derivatives and their numerical approximations. Sign Process 91(3):470–483
48. Valério D, da Costa JS (2013) An introduction to fractional control. IET, Stevenage. ISBN 978-1-84919-545-4
49. Wang Y, Pivonka P, Buenzli PR, Smith DW, Dunstan CR (2011) Computational modeling of interactions between multiple myeloma and the bone microenvironment. PloS one 6(11):e27494
50. Zumsande M, Stiefs D, Siegmund S, Gross T (2011) General analysis of mathematical models for bone remodeling. Bone 48(4):910–7